Direct observation of spin-polarised bulk bands in an inversion-symmetric semiconductor

J. M. Riley,[1] F. Mazzola,[2] M. Dendzik,[3] M. Michiardi,[3] T. Takayama,[4,5] L. Bawden,[1] C. Granerød,[2] M. Leandersson,[6] T. Balasubramanian,[6] M. Hoesch,[7] T. K. Kim,[7] H. Takagi,[4,5] W. Meevasana,[8,9] Ph. Hofmann,[3] M. S. Bahramy,[10,11] J. W. Wells,[2] and P. D. C. King[1,*]

[1]*SUPA, School of Physics and Astronomy, University of St. Andrews, St. Andrews, Fife KY16 9SS, United Kingdom*

[2]*Department of Physics, Norwegian University of Science and Technology (NTNU), N-7491 Trondheim, Norway*

[3]*Department of Physics and Astronomy, Interdisciplinary Nanoscience Center (iNANO), Aarhus University, 8000 Aarhus C, Denmark*

[4]*Department of Physics, University of Tokyo, Hongo, Tokyo 113-0033*

[5]*Max Planck Institute for Solid State Research, 70569 Stuttgart, Germany*

[6]*MAX IV Laboratory, Lund University, P. O. Box 118, 221 00 Lund, Sweden*

[7]*Diamond Light Source, Harwell Campus, Didcot, OX11 0DE, United Kingdom*

[8]*School of Physics, Suranaree University of Technology, Nakhon Ratchasima, 30000, Thailand*

[9]*NANOTEC-SUT Center of Excellence on Advanced Functional Nanomaterials, Suranaree University of Technology, Nakhon Ratchasima 30000, Thailand*

[10]*Quantum-Phase Electronics Center and Department of Applied Physics, The University of Tokyo, Tokyo 113-8656, Japan*

[11]*RIKEN center for Emergent Matter Science (CEMS), Wako 351-0198, Japan*

(Dated: August 8, 2014)

Methods to generate spin-polarised electronic states in non-magnetic solids are strongly desired to enable all-electrical manipulation of electron spins for new quantum devices.[1] This is generally accepted to require breaking global structural inversion symmetry.[1–5] In contrast, here we report the observation from spin- and angle-resolved photoemission spectroscopy of spin-polarised bulk states in the centrosymmetric transition-metal dichalcogenide WSe_2. Mediated by a lack of inversion symmetry in constituent structural units of the bulk crystal where the electronic states are localised,[6] we show how enormous spin splittings up to ~ 0.5 eV result, with a spin texture that is strongly modulated in both real and momentum space. Through this, our study provides direct experimental evidence for a putative locking of the spin with the layer and valley pseudospins in transition-metal dichalcogenides,[7,8] of key importance for using these compounds in proposed valleytronic devices.

The powerful combination of inversion symmetry $[E(\mathbf{k},\uparrow) = E(-\mathbf{k},\uparrow)]$ with time-reversal symmetry $[E(\mathbf{k},\uparrow) = E(-\mathbf{k},\downarrow)]$ ensures that electronic states of non-magnetic centrosymmetric materials must be doubly spin-degenerate. If inversion symmetry is broken, however, relativistic spin-orbit interactions can induce a momentum-dependent spin splitting via an effective magnetic field imposed by spatially-varying potentials. If the resulting spin polarisations can be controllably created and manipulated, they hold enormous promise to enable a range of new quantum technologies. These include routes towards electrical control of spin precession for spin-based electronics,[1,9] new ways to engineer topological states[10,11] and possible hosts of Majorana fermions for use in quantum computation.[5] There are two generally-accepted methods for stabilising spin-polarised states without magnetism, both exploiting breaking of global inversion symmetry. Structural inversion asymmetry can be created in a centrosymmetric host by imposing an electrostatic potential gradient, for example within an asymmetric quantum well, leading to Rashba-split[12] states localised at surfaces or interfaces.[13–16] Alternatively, a lack of global inversion symmetry in the unit cell can mediate spin splitting of the bulk electronic states, either through a Dresselhaus-type interaction,[17] or a recently discovered bulk form of the Rashba effect.[4,18]

Here, we present direct experimental evidence that $2H$-WSe_2, a material which retains bulk inversion symmetry, nonetheless exhibits a large spin polarisation of its bulk electronic states. This layered compound is composed of stacked Se-W-Se planes (Fig. 1(a)), each

of which contains an in-plane net dipole moment which is proposed to lead to a strong spin-valley coupling for an isolated monolayer.[19–21] The bulk unit cell contains two such monolayers, stacked in a staggered 'AB' configuration, restoring inversion symmetry and necessitating spin degeneracy of the bulk electronic states. Nevertheless, combining spin- and angle-resolved photoemission spectroscopy (ARPES) with electronic structure calculations, we observe a large layer- and momentum-dependent spin polarisation of these bulk bands.

We first summarise the bulk electronic structure of WSe_2 (Fig. 1). The material is known to be a semiconductor, consistent with our experimental observations where we find the Fermi level located within the band gap. We find the band extrema of the valence bands at Γ and K to be almost degenerate,[22] but here can resolve that the valence band maximum is located at the bulk Γ point, with significant dispersion of these zone-centre states along the surface normal (k_z) direction (Fig. 1(c,e)). Our measured band dispersions are in excellent agreement with those calculated from density-functional theory (DFT) (see also Supplementary Fig. S1), confirming that we are probing the bulk electronic states of WSe_2. The broad total bandwidth of more than 4 eV of the cosine-like upper valence bands along $\Gamma - A$ reflects the spatially extended nature of W $5d$ and Se $5p$ orbitals from which these states predominantly derive.

As well as these dispersive states we find a series of quasi-2D states, predominantly of planar $d_{x^2-y^2}$, d_{xy}, and $p_{x/y}$ orbital character (see Fig. 4(e)). The small overlap of these orbitals along the z direction, combined with suppressed interlayer hopping due to spin-orbit coupling,[7] results in minimal dispersion along k_z, while their extended nature in-plane ensures significant dispersion throughout the surface Brillouin zone (Fig. 1(d)). The lowest binding energy 2D states form a pair of hole-like bands centred at the Brillouin zone corners, contributing concentric almost circular pockets near the band top. These become trigonally warped as they grow in size with increasing binding energy, eventually merging with the zone-centre bands to form bone-shaped pockets centred at $\overline{M}$. The large splitting of $\sim$0.5 eV of the top of these bands at $\overline{K}$ signifies the strong atomic spin-orbit interaction in this compound, which is further reflected by our observation of hybridisation gaps, for example between two- and three-dimensional states along the $\Gamma - A$ line (Fig. 1(e)). Despite such strong spin-orbit coupling, we stress that all states remain spin-degenerate in our calculations, as expected from the bulk inversion symmetry of the crystal.

Intriguingly, however, our spin-resolved photoemission measurements reveal a strong spin

polarisation of the upper pair of valence band states at the $\overline{K}$ point of the Brillouin zone (Fig. 2). The measured polarisation is entirely out of the surface plane within experimental error, with up (down) orientation for the upper (lower) valence band, respectively. From fitting the measured energy distribution curves (EDCs, see methods), we estimate the magnitude of the spin polarisation to exceed 90%, suggestive of an almost fully spin-polarised band. Moreover, the sign of all polarisations are reversed at the $\overline{K'} = -\overline{K}$ point, confirming that time-reversal symmetry remains unbroken, and thus there is no net magnetic moment. This points to a non-magnetic origin of the observed spin polarisation, seemingly at odds with the centrosymmetric nature of the bulk crystal structure (Fig. 1(a)). We attribute this to the *local* inversion asymmetry of individual WSe_2 layers, leading to spin-polarised states whose texture is strongly modulated in both real and momentum space despite the global inversion symmetry of the unit cell. For these quasi-two-dimensional bands around $\overline{K}$, our calculations reveal that the electronic wavefunctions are almost completely localised on individual Se-W-Se layers of the bulk crystal. This is consistent with a spin-orbit mediated suppression of interlayer hopping predicted at the $\overline{K}$ point for bilayer WSe_2, which was proposed to lead to a strong coupling of the real spin with the layer pseudospin.[7] Such spin-layer locking was subsequently attributed as the origin of characteristic circularly and linearly polarised photoluminescence from bilayer WSe_2.[8]

As in the bilayer, with the electronic wavefunctions localised on a single Se-W-Se layer (half of the unit cell) of the bulk crystal around $\overline{K}$, the D_{6h} symmetry of the crystal is effectively reduced to D_{3h}, allowing a net dipole moment within the *ab*-plane (Fig. 1(a)). A recent theory has established the general grounds by which such a lack of inversion symmetry of the crystal site point group can lead to a macroscopic spin polarisation, driven by the local nature of spin-orbit coupling.[6] Indeed, our calculated *bulk* wavefunctions projected onto either WSe_2 layer of the unit cell are almost fully spin polarised for the topmost two valence bands at $\overline{K}$ (Fig. 2(g)). The 180° rotation of neighbouring layers in AB-stacked WSe_2, however, ensures that the sign of the spin polarisation is opposite between adjacent layers (Fig. 2(h)). This leads to a strong spin-layer locking,[7,8] with an overall spin degeneracy of the bulk electronic structure as required for a centrosymmetric material. Photoemission, being extremely surface sensitive, can be expected to predominantly probe the top layer of this material. We thus attribute the strong measured spin polarisation we observe here as a direct observation of a layer-localised spin-polarisation of bulk electronic states in WSe_2.

This is further supported by our photon-energy dependent measurements (Fig. 2(i)), which show how the measured photoelectron spin polarisation at $\overline{K}$ can be tuned nearly to zero. Our model calculations (see also Supplementary Fig. S3 and associated discussion) show how this arises due to the interference[23,24] of spin-up and spin-down polarised photoelectrons emitted from different layers of the material. This strongly supports our conclusions of a huge momentum-dependent spin splitting of up to $\sim$0.5 eV for bulk states localised in a constituent layer of the unit cell in WSe_2, with a spin orientation that is directly tied to the layer pseudospin. We note that the size of this observed spin splitting dramatically exceeds spin-orbit mediated splittings typically observed to date, even in surface Rashba systems with strong local in-plane field gradients.[14,25] This is because here, the energy of the spin splitting at the band extrema is directly set by the atomic spin-orbit coupling strength.[7]

Figure 3 reveals how the underlying spin-polarised states evolve along the $\overline{K} - \overline{\Gamma} - \overline{K'}$ direction. We find a dramatic suppression of the out-of-plane spin polarisation approximately half way along this line, with negligible polarisation observed around the zone centre. This is reproduced by our *ab-initio* calculations (Fig. 4(a)), and can be understood considering the orbital character of the underlying states (Fig. 4(e)). Close to $\overline{K}$, the electronic states are derived from mostly d_{xy} and $d_{x^2-y^2}$ orbitals. There is thus significant orbital overlap within the surface plane which, together with the net in-plane dipole, favours strong out-of-plane spin polarisation.[26] Around $\overline{\Gamma}$, however, the orbital character becomes dominantly d_{z^2}/p_z-like, causing this component to be strongly suppressed, as found experimentally, while also driving the observed increase in dimensionality of the electronic states. Intriguingly, we also find a small in-plane spin component emerges along $\overline{K'} - \overline{\Gamma} - \overline{K}$, which again switches sign either side of $\overline{\Gamma}$. This component would not naively be expected given the symmetry of the Se-W-Se layer, which has no net dipolar field along the out-of-plane direction, which we have confirmed by explicit slab calculations for an ideal bulk-like termination. The emergence of this component therefore reflects additional complexity beyond that considered in our theoretical approach, such as small surface relaxations leading to a non-negligible contribution of the dipole out of the surface plane. We stress, however, that this has only a small effect and the predominant contribution to the strong out-of-plane spin polarisations observed here are intrinsic to the bulk electric structure.

We additionally find a suppression of this out-of-plane spin polarisation along the entire

$\overline{M}-\overline{\Gamma}$ direction. Unlike at the zone centre, however, this cannot be attributed to a change in orbital character: The electronic states close to $\overline{M}$ are predominantly derived from planar orbitals, similar to around $\overline{K}$, and we accordingly find strong layer-resolved spin polarisations of the underlying bands close to $\overline{M}$ (Fig. 4). Rather, the suppression of spin polarisation along $\overline{M}-\overline{\Gamma}$ is mediated by the degeneracy of two oppositely polarised bands within a single layer. At the $\overline{M}$ point itself, this is a natural consequence of time-reversal symmetry, as $\overline{M}$ is a time-reversal invariant momentum. Along the $\overline{M}-\overline{\Gamma}$ line, such degeneracies are enforced by the combination of time-reversal with the rotational D_{3h} symmetry of a single monolayer within the unit cell, ensuring that the out-of-plane component of the spin must have opposite sign in neighbouring sextants of the Brillouin zone.

Together, our calculations and experiment thus point to an extremely rich real- and momentum-space dependent spin texture of bulk transition-metal dichalcogenides. They provide a direct demonstration of a pronounced coupling between the spin, valley, and layer degrees of freedom, of key importance to widespread proposals to utilise these materials in exotic devices exploiting the valley pseudospin.[7,8,19–21,27–29] More generally, our experimental measurement of spin-polarised bulk electronic states in a centrosymmetric material opens a wealth of new opportunities for creating, probing, and controlling spin and valley polarisation in bulk solids via local inversion asymmetry.

Methods

ARPES: ARPES measurements were performed at the I05 beamline of Diamond Light Source, UK, and spin-ARPES measurements at the I3 beamline of MAX-III synchrotron, Sweden.[30] Single crystal samples of WSe_2, grown by the chemical vapour transport method, were cleaved *in-situ* and measured at temperatures ranging from 30-300 K. Measurements were performed using p-polarised synchrotron light from 20-130 eV (ARPES) and 20-40 eV (spin-ARPES), and employing Scienta R4000 hemispherical electron analysers. For the spin-ARPES measurements, a mini-Mott detector scheme was utilised, permitting simultaneous detection of the out-of-plane and one in-plane (along the analyser slit direction) component of the photoelectron spin.[30] A Sherman function of $S = 0.17$ was used to generate the measured spin polarisations,[30]

$$P_i = \frac{(I_i^+ - I_i^-)}{S(I_i^+ + I_i^-)},$$

where P_i is the photoelectron spin polarisation measured along the out-of-plane, $i = \perp$, or in-plane, $i = \parallel$, direction, and $I_i^{\pm}$ is the measured intensity on the individual detectors in the Mott

scattering chamber, corrected by a relative detector efficiency calibration. To extract numerical values of the polarisation, we fitted the measured EDCs to two Lorentzian peaks and a Shirley background, convolved with a Gaussian function to account for the instrumental resolution, with the corresponding Lorentzian peak areas used to derive the measured spin polarisation. We also applied a geometrical correction to account for the finite angle between the sample and the electron spectrometer, and the corresponding influence of this on the spin polarisation measured in the reference frame of the spectrometer. To determine the k_z dispersion from photon-energy dependent ARPES, we employed a free electron final state model

$$k_z = \sqrt{2m_e/\hbar^2}(V_0 + E_{\rm k}\cos^2\theta)^{1/2},$$

where θ is the in-plane emission angle and V_0 is the inner potential. Our photon energy range covers more than 6 complete Brillouin zones along k_z, and we find best agreement taking an inner potential of 13 eV and a c-axis lattice constant of 13.45 Å.

Calculations: Electronic structure calculations were performed within the context of density functional theory (DFT) using the modified Becke-Johnson exchange potential and Perdew-Burke-Ernzerhof correlation functional as implemented in the WIEN2K programme.[31] Relativistic effects, including spin-orbit coupling, were fully included. The Brillouin zone was sampled by a 12x12x6 k-mesh. For the orbital and layer projection calculation, a tight binding Hamiltonian for the bulk band structure was constructed by downfolding the DFT results using maximally localised Wannier functions,[32–34] employing as a basis W $5d$ and $5s$ orbitals and Se $5p$ and $5s$ orbitals.

---

* To whom correspondence should be addressed: philip.king@st-andrews.ac.uk

[1] Koo, H. C. *et al.* Control of Spin Precession in a Spin-Injected Field Effect Transistor. *Science* **325**, 1515-1518 (2009).

[2] Hsieh, D. *et al.* A Topological Dirac Insulator in a Quantum Spin Hall Phase. *Nature* **452**, 970-974 (2008).

[3] Bahramy, M. *et al.* Emergent Quantum Confinement at Topological Insulator Surfaces. *Nature Commun.* **3**, 1159 (2012).

[4] Murakawa, H. *et al.* Detection of Berry's Phase in a Bulk Rashba Semiconductor. *Science* **342**, 1490–1493 (2013).

[5] Mourik, V. *et al.* Signatures of Majorana Fermions in Hybrid Superconductor-Semiconductor Nanowire Devices. *Science* **336**, 1003–1007 (2012).

[6] Zhang, X., Liu, Q., Luo, J. W., Freeman, A. J. & Zunger, A. Hidden Spin Polarization in Inversion-Symmetric Bulk Crystals. *Nature Phys.* **10**, 387–393 (2014).

[7] Gong, Z., *et al.* Magnetoelectric effects and valley-controlled spin quantum gates in transition metal dichalcogenide bilayers. *Nature Commun.* **4**, 2053 (2013).

[8] Jones, A. M., *et al.* Spin-layer locking effects in optical orientation of exciton spin in bilayer WSe_2. *Nature Phys.* **10**, 130–134 (2014).

[9] Datta, S. & Das, B. Electronic Analog of the Electro-Optic Modulator. *Appl. Phys. Lett.* **56**, 665-667 (1990).

[10] Das, T. & Balatsky, A. V. Engineering Three-Dimensional Topological Insulators in Rashba-Type Spin-Orbit Coupled Heterostructures. *Nature Commun.* **4**, 1972 (2013).

[11] Zhou, J. J., Feng, W., Zhang, Y., Yang, S. A. & Yao, Y. Engineering Topological Surface States and Giant Rashba Spin Splitting in BiTeI/Bi_2Te_3 Heterostructures. *Sci. Rep.* **4**, 3841 (2014).

[12] Bychkov, Y. A. & Rashba, E. I. Properties of a 2D Electron Gas with Lifted Spectral Degeneracy. *JETP Lett.* **39**, 78-81 (1984).

[13] Nitta, J., Akazaki, T., Takayanagi, H. & Enoki, T. Gate Control of Spin-Orbit Interaction in an Inverted $In_{0.53}Ga_{0.47}As/In_{0.52}Al_{0.48}As$ Heterostructure. *Phys. Rev. Lett.* **78**, 1335–1338 (1997).

[14] Ast, C. R. *et al.* Giant Spin Splitting through Surface Alloying. *Phys. Rev. Lett.* **98**, 186807 (2007).

[15] King, P. D. C. *et al.* Large Tunable Rashba Spin Splitting of a Two-Dimensional Electron Gas in Bi_2Se_3. *Phys. Rev. Lett.* **107**, 096802 (2011).

[16] King, P. D. C. *et al.* Quasiparticle Dynamics and Spin-Orbital Texture of the $SrTiO_3$ Two-Dimensional Electron Gas. *Nature Commun.* **5**, 3414 (2014).

[17] Dresselhaus, G. Spin-Orbit Coupling Effects in Zinc Blende Structures. *Phys. Rev.* **100**, 580-586 (1955).

[18] Ishizaka, K. *et al.* Giant Rashba-Type Spin Splitting in Bulk BiTeI. *Nature Mat.* **10**, 521–526 (2011).

[19] Xiao, D., Liu, G.-B., Feng, W., Xu, X. & Yao, W. Coupled Spin and Valley Physics in

Monolayers of MoS_2 and Other Group-VI Dichalcogenides. *Phys. Rev. Lett.* **108**, 196802 (2012).

[20] Mak, K. F., He, K., Shan, J. & Heinz, T. F. Control of Valley Polarization in Monolayer MoS_2 by Optical Helicity. *Nature Nano.* **7**, 494–498 (2012).

[21] Zeng, H., Dai, J., Yao, W., Xiao, D. & Cui, X. Valley Polarization in MoS_2 Monolayers by Optical Pumping. *Nature Nano.* **7**, 490–493 (2012).

[22] Finteis, T. *et al.* Occupied and Unoccupied Electronic Band Structure of WSe_2. *Phys. Rev. B* **55**, 10400–10411 (1997).

[23] Zhu, Z.-H. *et al.* Layer-by-Layer Entangled Spin-Orbital Texture of the Topological Surface State in Bi_2Se_3. *Phys. Rev. Lett.* **110**, 216401 (2013).

[24] Zhu, Z.-H. *et al.* Photoelectron Spin-Polarization Control in the Topological Insulator Bi_2Se_3. *Phys. Rev. Lett.* **112**, 076802 (2014).

[25] Bihlmayer, G. *et al.* Enhanced Rashba spin-orbit splitting in Bi/Ag(111) and Pb/Ag(111) surface alloys from first principles. *Phys. Rev. B* **75**, 195414 (2007).

[26] Yuan, H. *et al.* Zeeman-Type Spin Splitting Controlled by an Electric Field. *Nature Phys.* **9**, 563–569 (2013).

[27] Jones, A. M. *et al.* Optical Generation of Excitonic Valley Coherence in Monolayer WSe_2. *Nature Nano.* **8**, 634–638 (2013).

[28] Zhang, Y. J., Oka, T., Suzuki, R., Ye, J. T. & Iwasa, Y. Electrically Switchable Chiral Light-Emitting Transistor. *Science* **344**, 725–728 (2014).

[29] Xu, X., Yao, W., Xiao, D. & Heinz, T. F. Spin and Pseudospins in Layered Transition Metal Dichalcogenides. *Nature Phys.* **10**, 343-350 (2014).

[30] Berntsen, M. H. *et al.* A Spin- and Angle-Resolving Photoelectron Spectrometer. *Rev. Sci. Instrum.* **81**, 035104 (2010).

[31] Blaha, P. et al., WIEN2K package, Version 10.1 (2010); available at, http://www.wien2k.at.

[32] Souza, I. *et al.* Maximally Localized Wannier Functions for Entangled Energy Bands. *Phys. Rev. B* **65**, 035109 (2001).

[33] Mostofi, A. A. *et al.* Wannier90: A Tool for Obtaining Maximally Localised Wannier Functions. *Comp. Phys. Commun.* **178**, 685699 (2008).

[34] Kuneš, J. *et al.* WIEN2WANNIER: From Linearized Augmented Plane Waves to Maximally Localized Wannier Functions. *Comp. Phys. Commun.* **181**, 18881895 (2010).

Acknowledgements

We gratefully acknowledge support from the Engineering and Physical Sciences Research Council, UK, the VILLUM foundation, the Calipso program, TRF-SUT Grant RSA5680052 and NANOTEC, Thailand through the CoE Network. PDCK acknowledges support from the Royal Society through a University Research Fellowship. MSB was supported by the Grant-in-Aid for Scientific Research (S) (No. 24224009) from the Ministry of Education, Culture, Sports, Science and Technology (MEXT) of Japan. The experiments at the MAX IV Laboratory were made possible through funding from the Swedish Research Council and the Knut and Alice Wallenberg Foundation.

Author contributions: The experimental data was measured by JMR, FM, MD, MM, LB, CG, WM, JWW, and PDCK and analysed by JMR, FM, JWW and PDCK. MSB performed the electronic structure calculations. TT grew the samples. ML and TB, and MH and TKK maintained the spin-ARPES and ARPES end stations, respectively, and provided experimental support. PDCK, JWW, MSB, PH, and HT provided the project infrastructure. All authors discussed the results and their interpretation. PDCK and JMR wrote the manuscript with input and discussion from all co-authors. PDCK was responsible for overall project planning and direction.

Additional Information: The authors declare no competing financial interests. Supplementary information accompanies this paper at www.nature.com/naturephysics. Reprints and permission information is available online at http://npg.nature.com/reprintsandpermissions/. Correspondence and requests for materials should be addressed to P.D.C.K.

Figure Captions:

FIG. 1: **Bulk electronic structure of WSe_2.** (a) Side and top views of the bulk crystal structure of WSe_2. The unit cell contains two Se-W-Se units in which there is a net in-plane dipole pointing to the right and left, respectively. (b) Corresponding bulk and surface Brillouin zone. ARPES measurements ($h\nu$ = 125 eV, T = 30 K) of (c) the electronic structure along the $\overline{K'} - \overline{\Gamma} - \overline{K}$ direction and (d) isoenergy contours throughout the surface Brillouin zone, reveal sharply-defined bands (for example the upper valence bands at $\overline{K}$) with significant in-plane dispersion, indicative of two-dimensional electronic states. We also observe broader "filled-in" pockets of spectral weight characteristic of three-dimensional states, where the finite k_z resolution of ARPES leads to broadening. (e) We directly confirm this absence or presence, respectively, of significant k_z dispersion from photon energy-dependent ARPES measurements (see also methods and Supplementary Fig. S1). Our measured electronic structure is in excellent agreement with that calculated from density-functional theory (solid lines in (c) and (e)), confirming that we are probing the bulk electronic states of WSe_2.

FIG. 2: **Observation of spin-polarised bulk bands in an inversion symmetric host.** Energy distribution curves from spin-resolved ARPES measurements ($h\nu = 25$ eV, $T = 300$ K) at the $\overline{K}$ point measured by the (a) out-of-plane ($I_\perp$) and (b) in-plane ($I_\parallel$) detectors in the Mott scattering chamber (corresponding measurements correcting for the finite Mott-detector efficiencies are shown in Supplemental Fig. S2). (c) The extracted polarisations show a strong out-of-plane spin polarisation, opposite for the two valence band peaks. (d-f) The signs of all components are reversed at the $\overline{K'}$ point. (g) Our projection of the calculated bulk band structure onto the first layer of the unit cell reveals a strong spin polarisation of electronic bands localised on this layer (e.g. at $\overline{K}$), whose sign is reversed in the second layer of the unit cell as shown in (h). The measured spin polarisation at $\overline{K}$ exhibits a strong photon energy dependence (i). Error bars reflect an approximate estimate of the uncertainty in extracting the polarisation from the experimental measurements, incorporating statistical errors in peak fitting, systematic errors and uncertainty in sample alignment. Our model calculations (solid line, see Supplementary Information), reveal how this occurs due to interference between outgoing photoelectrons originating from the different layers of the crystal.

FIG. 3: **Evolution of spin texture along $\overline{K'}-\overline{\Gamma}-\overline{K}$.** (a) Dispersion measured by ARPES ($h\nu =$ 125 eV, $T = 30$ K), along the $\overline{K'}-\overline{\Gamma}-\overline{K}$ direction. Vertical lines mark the locations of the EDCs measured using spin-resolved photoemission ($h\nu = 25$ eV, $T = 300$ K), and corresponding extracted spin polarisations, shown in (b)–(e). (f) The out-of- ($P_\perp$) and in- ($P_\parallel$) plane spin polarisations determined from fitting these and additional EDCs ($h\nu = 25$ eV, $T = 80$ K [squares and vertical diamonds, respectively] and $T = 300$ K [circles and horizontal diamonds, respectively]) reveal some canting of the spin into the surface plane away from the $\overline{K}$ points, and a total suppression of the measured spin polarisation around the zone centre. Error bars reflect an approximate estimate of the uncertainty in extracting the polarisation from the experimental measurements, incorporating statistical errors in peak fitting, systematic errors and uncertainty in sample alignment. The lines in (f) are provided as guides to the eye.

FIG. 4: **Momentum-dependent suppression of layer-resolved spin polarisation.** (a) Momentum-dependence of the out-of-plane spin polarisation of the top two valence bands throughout the Brillouin zone, calculated for the $k_z = 0$ plane and projected onto the first Se-W-Se layer of the unit cell. White regions indicate suppression of the layer-resolved spin-polarisation. At the $\overline{M}$ point, our (b) ARPES measurements ($h\nu = 125$ eV, $T = 30$ K) and corresponding spin polarisation determined from spin-ARPES ($h\nu = 25$ eV, $T = 300$ K) along the coloured (c) MDC and (d) EDC show how this occurs through the crossing of strongly spin-polarised bands. In contrast, towards the zone centre, our orbitally-projected band structure calculations (e) reveal how this is correlated with the emergence of significant out-of-plane orbital character of the electronic states.

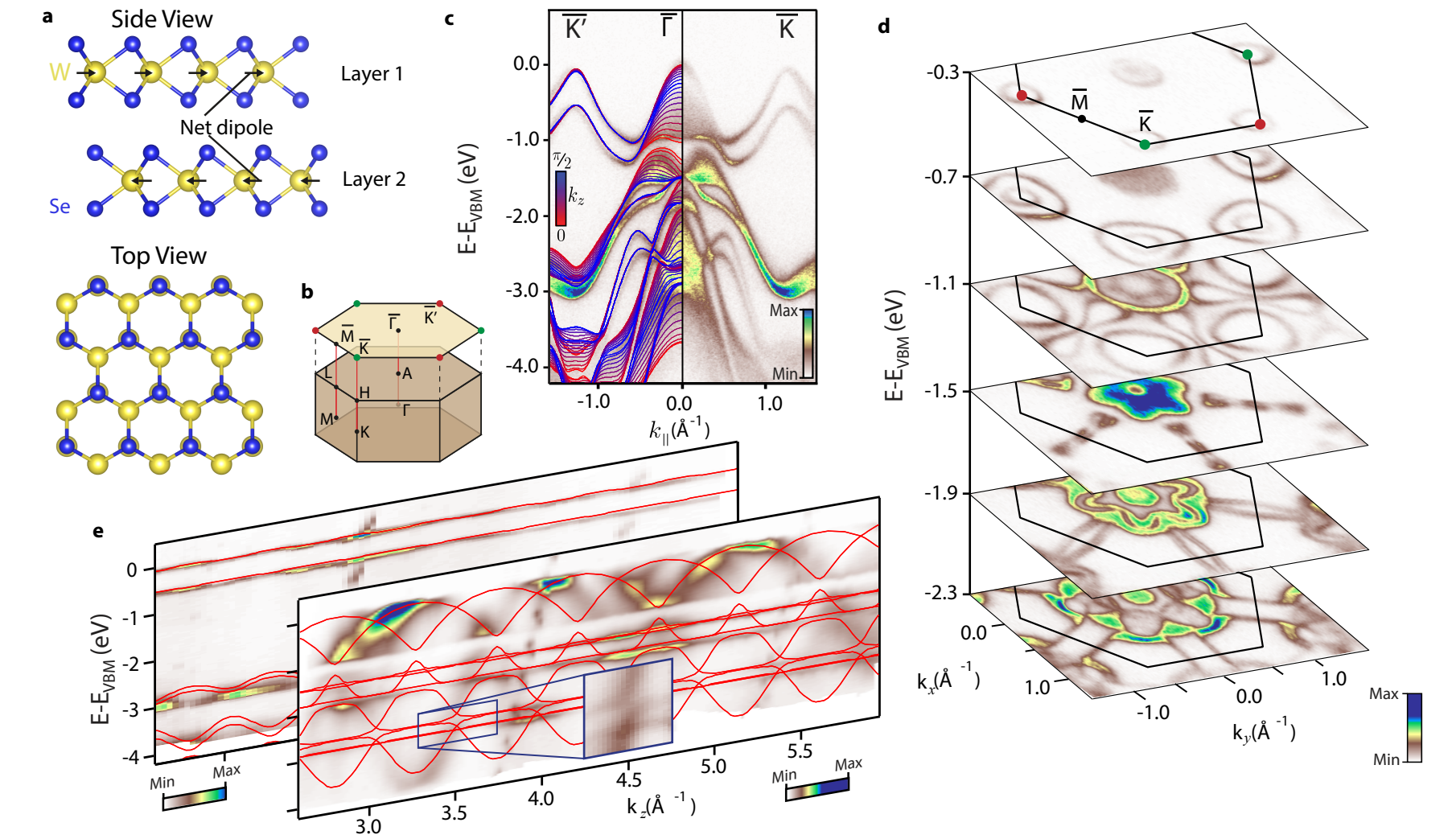
a
Side View
W
Layer 1
Net dipole
Layer 2
Se
Top View
b
K'
Γ
K
M
L
A
H
c
K'
Γ
K
0.0
-1.0
-2.0
-3.0
-4.0
E-E_VBM (eV)
π/2
k_z
0
Max
Min
-1.0
0.0
1.0
k_∥(Å^-1)
d
-0.3
-0.7
-1.1
-1.5
-1.9
-2.3
M
K
E-E_VBM (eV)
0.0
1.0
k_x(Å^-1)
-1.0
0.0
1.0
k_y(Å^-1)
Max
Min
e
0
-1
-2
-3
-4
E-E_VBM (eV)
Min
Max
3.0
3.5
4.0
4.5
5.0
5.5
k_z(Å^-1)
Min
Max

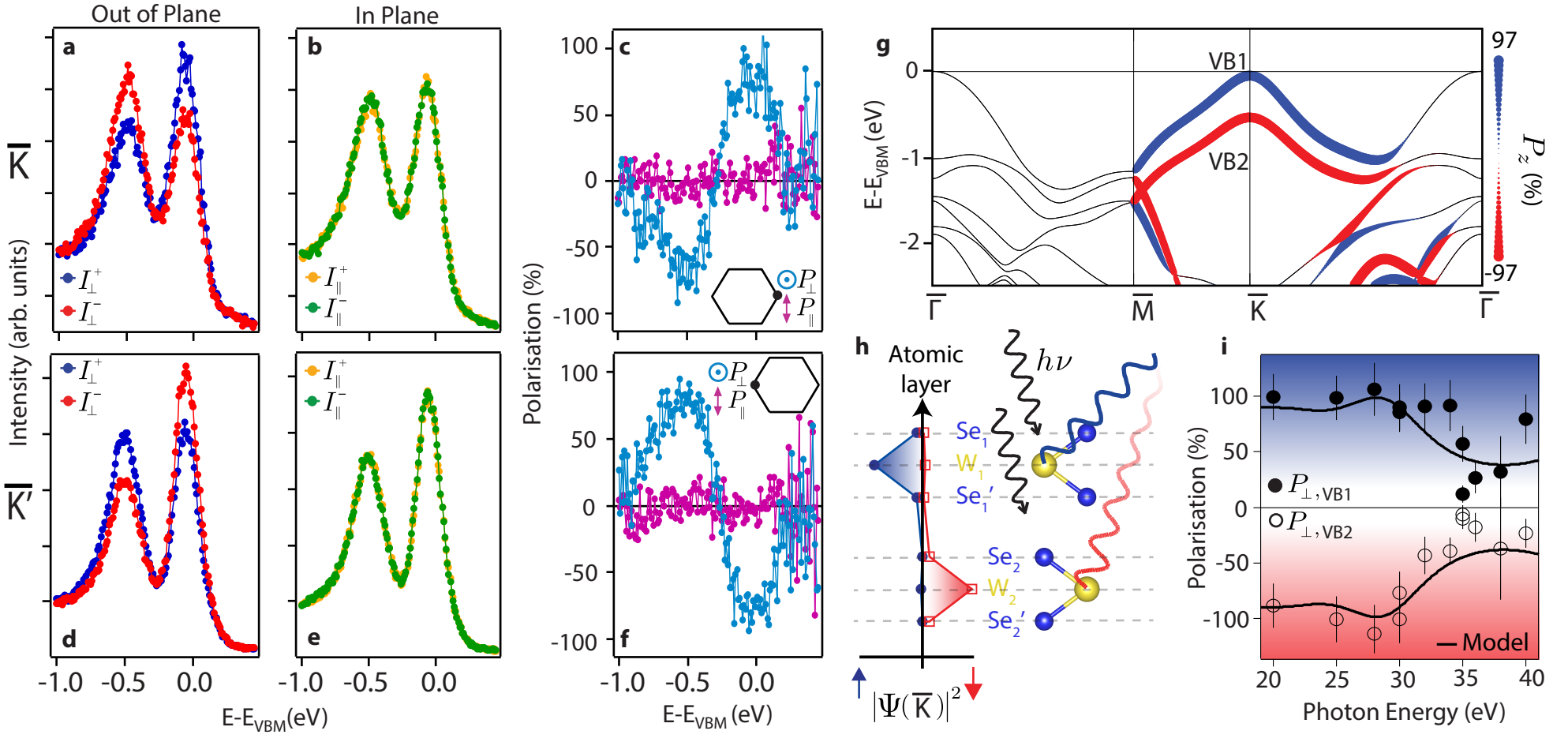
Out of Plane
In Plane
a
b
c
d
e
f
g
h
i
K
K'
Intensity (arb. units)
$I_\perp^+$
$I_\perp^-$
$I_\parallel^+$
$I_\parallel^-$
E-E$_{VBM}$(eV)
Polarisation (%)
$P_\perp$
$P_\parallel$
VB1
VB2
E-E$_{VBM}$ (eV)
P_z (%)
Γ̄
M̄
K̄
Atomic layer
$h\nu$
Se$_1$
W$_1$
Se$_1$′
Se$_2$
W$_2$
Se$_2$′
$|\Psi(\bar{K})|^2$
$P_{\perp,VB1}$
$P_{\perp,VB2}$
Model
Photon Energy (eV)

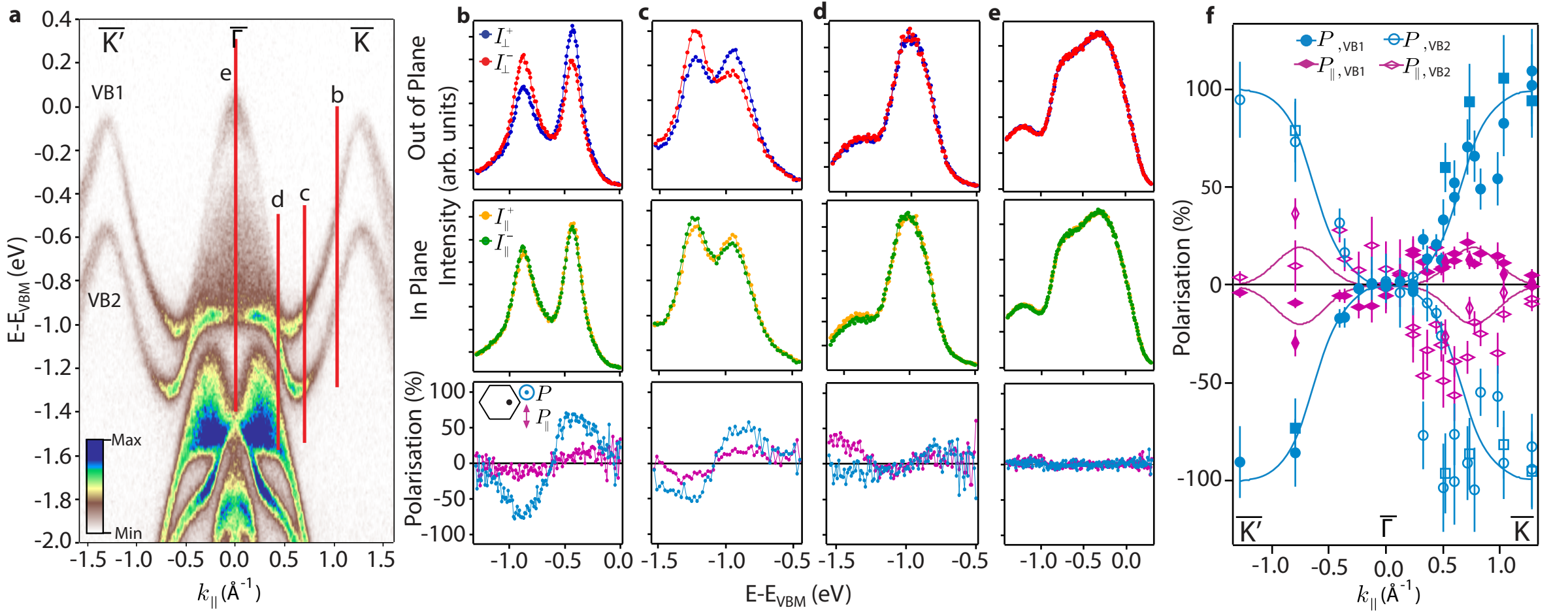
a
K′
Γ̄
K̄
VB1
VB2
e
d
c
b
Max
Min
E-E_VBM (eV)
k_|| (Å^-1)
b
c
d
e
Out of Plane
In Plane
Intensity (arb. units)
Polarisation (%)
E-E_VBM (eV)
f
P_⊥,VB1
P_⊥,VB2
P_||,VB1
P_||,VB2
Polarisation (%)
k_|| (Å^-1)

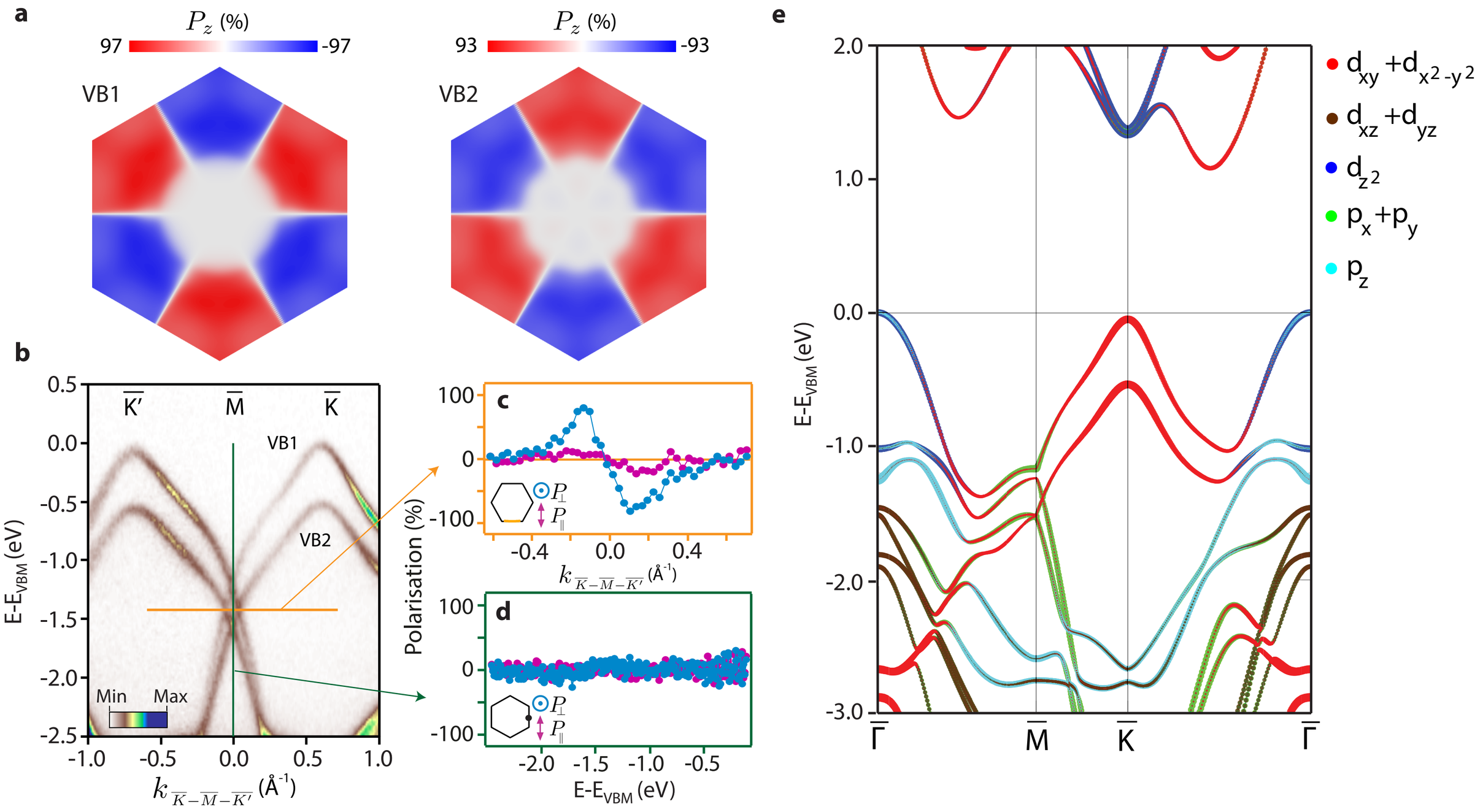
a
P_z (%)
97
-97
VB1
P_z (%)
93
-93
VB2
b
K′
M
K
VB1
VB2
Min
Max
E-E$_{VBM}$ (eV)
$k_{\overline{K}-\overline{M}-\overline{K'}}$ (Å^{-1})
c
d
Polarisation (%)
$P_\perp$
$P_\parallel$
E-E$_{VBM}$ (eV)
e
d_{xy} +$d_{x^2-y^2}$
d_{xz} +d_{yz}
d_{z^2}
p_x +p_y
p_z
E-E$_{VBM}$ (eV)
Γ
M
K
Γ

Supplementary Information: Direct observation of spin-polarised bulk bands in an inversion-symmetric semiconductor

J. M. Riley,[1] F. Mazzola,[2] M. Dendzik,[3] M. Michiardi,[3] T. Takayama,[4,5]
L. Bawden,[1] C. Granerød,[2] M. Leandersson,[6] T. Balasubramanian,[6]
M. Hoesch,[7] T. K. Kim,[7] H. Takagi,[4,5] W. Meevasana,[8,9]
Ph. Hofmann,[3] M. S. Bahramy,[10,11] J. W. Wells,[2] and P. D. C. King[1,*]

[1]*SUPA, School of Physics and Astronomy, University of St. Andrews, St. Andrews, Fife KY16 9SS, United Kingdom*

[2]*Department of Physics, Norwegian University of Science and Technology (NTNU), N-7491 Trondheim, Norway*

[3]*Department of Physics and Astronomy, Interdisciplinary Nanoscience Center (iNANO), Aarhus University, 8000 Aarhus C, Denmark*

[4]*Department of Physics, University of Tokyo, Hongo, Tokyo 113-0033*

[5]*Max Planck Institute for Solid State Research, 70569 Stuttgart, Germany*

[6]*MAX IV Laboratory, Lund University, P. O. Box 118, 221 00 Lund, Sweden*

[7]*Diamond Light Source, Harwell Campus, Didcot, OX11 0DE, United Kingdom*

[8]*School of Physics, Suranaree University of Technology, Nakhon Ratchasima, 30000, Thailand*

[9]*NANOTEC-SUT Center of Excellence on Advanced Functional Nanomaterials, Suranaree University of Technology, Nakhon Ratchasima 30000, Thailand*

[10]*Quantum-Phase Electronics Center and Department of Applied Physics, The University of Tokyo, Tokyo 113-8656, Japan*

[11]*RIKEN center for Emergent Matter Science (CEMS), Wako 351-0198, Japan*

(Dated: July 22, 2014)

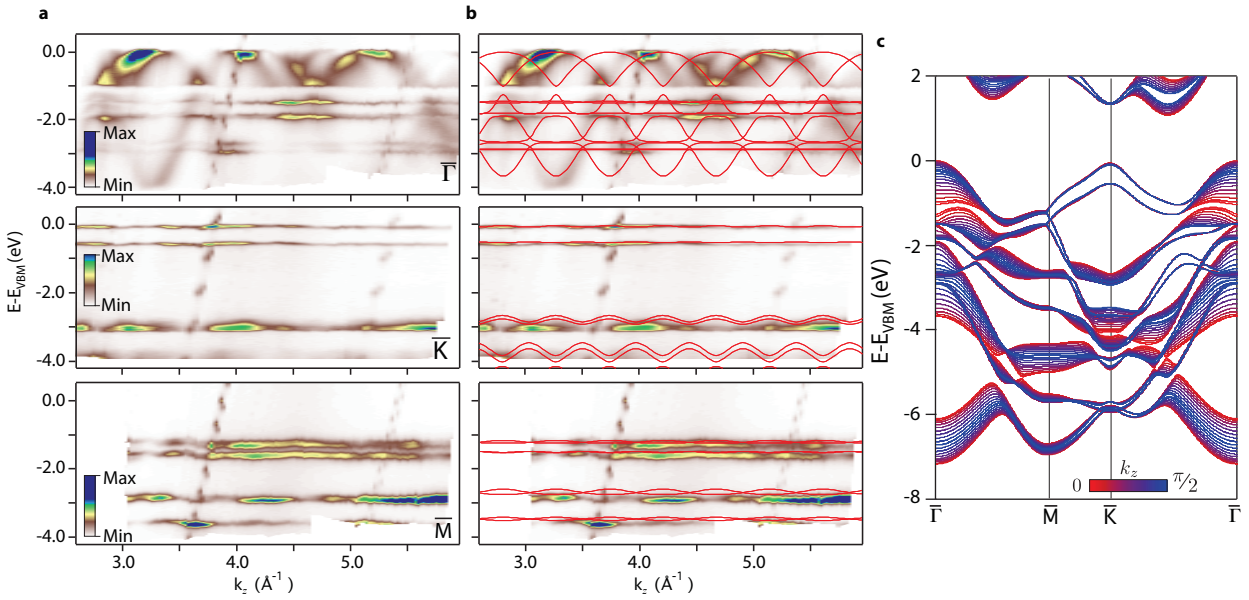

FIG. S1: k_z **dependence of bulk electronic structure of** WSe_2**.** (a) ARPES measurements of the k_z dispersion of electronic states at the $\overline{\Gamma}$, $\overline{K}$, and $\overline{M}$ points, respectively. The features which appear to form sharp diagonal lines are an experimental artefact arising from higher-order light. (b) Our *ab-initio* calculations are additionally included (red lines), showing good agreement with the measured dispersions. (c) The calculated electronic structure, shown projected onto the surface Brillouin zone for different values of k_z (coloured lines), indicates significant in-plane dispersion of all states, with the presence (absence) of substantial k_z dispersion for the different bands, characteristic of their three (two-) dimensional character, respectively.

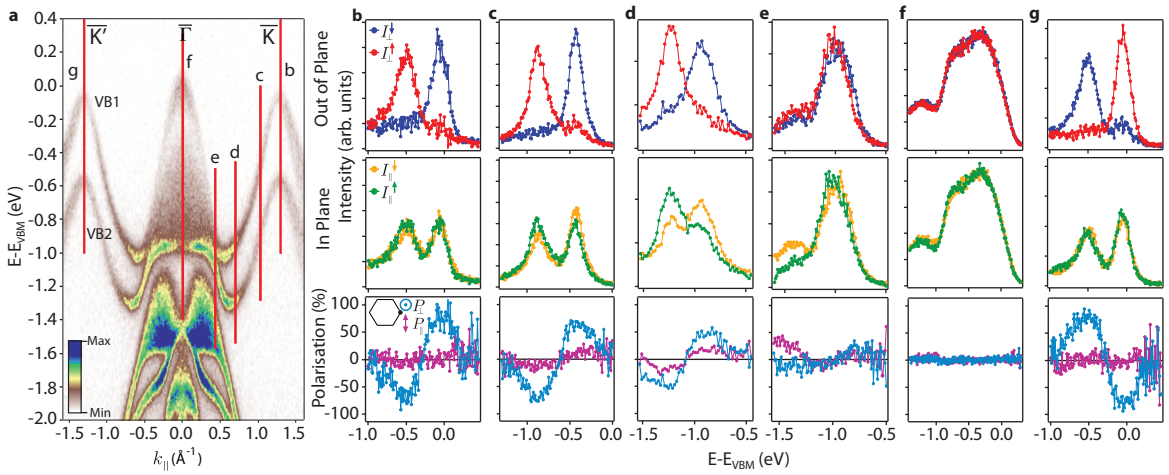

FIG. S2: **Spin-resolved EDCs.** (a) Dispersion measured by ARPES ($h\nu = 125$ eV, $T = 30$ K), along the $\overline{K'}-\overline{\Gamma}-\overline{K}$ direction. (b-g) Spin-resolved EDCs ($h\nu = 25$ eV, $T = 300$ K, measured along the red cuts in (a)), accounting for the finite efficiency of the spin detection (Sherman function of the Mott detectors). Here, $I_i^{\uparrow} = I_i^{tot}(1+P)/2$ and $I_i^{\downarrow} = I_i^{tot}(1-P)/2$, with $I_i^{tot} = (I_I^+ + I_i^-)$, $I_i^{\pm}$ as shown in the main text, $i = \{\perp, \|\}$, and the polarisation P_i shown in the bottom row, calculated as defined in the methods section.

2-LAYER MODEL FOR PHOTOELECTRON SPIN POLARISATION

To simulate the photon energy dependence of the measured spin polarisation by spin-resolved ARPES, shown in Fig. 2(i) of the main text, we start with a minimal model for the electronic structure of the upper valence band at $\overline{K}$, as used in Ref. 1:

$$\begin{aligned}
|\mathrm{VB1}\rangle \;=\; & \frac{\cos\alpha}{\sqrt{2}}\left[\left(\left|d^{\ell}_{x^2-y^2}\right\rangle + i\left|d^{\ell}_{xy}\right\rangle\right)\otimes|\uparrow\rangle + \left(\left|d^{u}_{x^2-y^2}\right\rangle - i\left|d^{u}_{xy}\right\rangle\right)\otimes|\downarrow\rangle\right] \\
& + \frac{\sin\alpha}{\sqrt{2}}\left[\left(\left|d^{u}_{x^2-y^2}\right\rangle - i\left|d^{u}_{xy}\right\rangle\right)\otimes|\uparrow\rangle + \left(\left|d^{\ell}_{x^2-y^2}\right\rangle + i\left|d^{\ell}_{xy}\right\rangle\right)\otimes|\downarrow\rangle\right] \qquad \text{(S1)} \\
= \; & \sum_{i,\sigma} c_i^{\sigma}\phi_{i,\sigma}, \qquad \text{(S2)}
\end{aligned}$$

where $i = u, \ell$ is the layer index for the upper and lower layer in the unit cell, respectively, and σ the spin index with

$$\begin{aligned}
c_u^{\uparrow} \;&=\; \frac{\sin\alpha}{\sqrt{2}} = c_{\ell}^{\downarrow} \\
c_u^{\downarrow} \;&=\; \frac{\cos\alpha}{\sqrt{2}} = c_{\ell}^{\uparrow} \\
\phi_{u,\uparrow\downarrow} \;&=\; \left|d^{u}_{x^2-y^2}\right\rangle - i\left|d^{u}_{xy}\right\rangle \\
\phi_{\ell,\uparrow\downarrow} \;&=\; \left|d^{\ell}_{x^2-y^2}\right\rangle + i\left|d^{\ell}_{xy}\right\rangle . \qquad \text{(S3)}
\end{aligned}$$

We take $\cos(2\alpha) = 0.9$ such that each layer is 90% spin polarised. We proceed to calculate the photoelectron spin polarisation following the method introduced in Refs. 2 and 3. We write the matrix element for photoemission, assuming plane wave final states, as

$$M_{\mathrm{VB1}} = \left\langle e^{i\mathbf{k}\cdot\mathbf{r}}\right| \mathbf{A}\cdot\mathbf{p}\,|\mathrm{VB1}\rangle = \sum_{i,\sigma} c_i^{\sigma} m_i, \qquad \text{(S4)}$$

where

$$\begin{aligned}
m_i \;&=\; \left\langle e^{i\mathbf{k}\cdot\mathbf{r}}\right| \mathbf{A}\cdot\mathbf{p}\,|\phi_i\rangle \\
&=\; e^{-ik_z z_i} e^{-z_i/(2\lambda\cos\theta)} \left\langle e^{i\mathbf{k}_{\parallel}\cdot\mathbf{r}_{\parallel}}\right| \mathbf{A}\cdot\mathbf{p}\,|\phi_i\rangle , \qquad \text{(S5)}
\end{aligned}$$

explicitly incorporating the effects of a layer-dependent phase and exponential attenuation of photoelectrons emitted from deeper atomic layers in the crystal, taking

$$k_z = \sqrt{\frac{2m_e}{\hbar^2}(h\nu - E_B) - k_{\parallel}^2}, \qquad \text{(S6)}$$

θ as the photoelectron emission angle for the $\overline{K}$ point, λ the inelastic mean free path, and z_i the layer spacing of W planes along the c-axis.

From the Pauli spin matrix

$$\sigma_z = \frac{\hbar}{2}\begin{pmatrix} 1 & 0 \\ 0 & -1 \end{pmatrix}, \tag{S7}$$

the z-component of the photoelectron spin polarisation is given by

$$P_z = \frac{I^{\uparrow} - I^{\downarrow}}{I^{\uparrow} + I^{\downarrow}} \tag{S8}$$

where

$$I^{\sigma} = \left| \sum_i c_i^{\sigma} m_i \right|^2 . \tag{S9}$$

Substituting Eqn. S9 into Eqn. S8, we get

$$P_z = \frac{\sum\limits_i \left(c_i^{\uparrow *} c_i^{\uparrow} - c_i^{\downarrow *} c_i^{\downarrow} \right) |m_i|^2 + \sum\limits_{i \neq i'} \left(c_i^{\uparrow *} c_{i'}^{\uparrow} - c_i^{\downarrow *} c_{i'}^{\downarrow} \right) m_i^* m_{i'}}{\sum\limits_i \left(c_i^{\uparrow *} c_i^{\uparrow} + c_i^{\downarrow *} c_i^{\downarrow} \right) |m_i|^2 + \sum\limits_{i \neq i'} \left(c_i^{\uparrow *} c_{i'}^{\uparrow} + c_i^{\downarrow *} c_{i'}^{\downarrow} \right) m_i^* m_{i'}}, \tag{S10}$$

where the latter terms give rise to interference between the layers. Taking only two layers, substituting Eqn. S3 and assuming $\left\langle e^{i\mathbf{k}_{\parallel}\cdot\mathbf{r}_{\parallel}} \right| \mathbf{A}\cdot\mathbf{p} \left| \phi_u \right\rangle = \left\langle e^{i\mathbf{k}_{\parallel}\cdot\mathbf{r}_{\parallel}} \right| \mathbf{A}\cdot\mathbf{p} \left| \phi_\ell \right\rangle$, Eqn. S10 simplifies to

$$P_z = \frac{\left(\sin^2\alpha - \cos^2\alpha\right)\left(1 - e^{-c/2\lambda\cos\theta}\right)}{1 + e^{-c/2\lambda\cos\theta} + 4\sin\alpha\cos\alpha\cos\left(\frac{k_z c}{2}\right) e^{-c/4\lambda\cos\theta}}. \tag{S11}$$

An oscillatory dependence of the measured photoelectron spin polarisation on photon energy is clearly apparent from the $\cos\left(\frac{k_z c}{2}\right)$ term, qualitatively supporting our assignment of the decrease of the measured photoelectron spin polarisation at photon energies around 35 eV (Fig. 2(i) of the main text) to an interference effect.

To further validate this conclusion, we numerically solve Eqn. S10 for a 20-layer bulk-like model, taking inelastic mean free paths as calculated from the TPP-2M predictive formula [4], although we note that we find similar results for fixed inelastic mean free paths on the order of 5 Å, and assuming a photon energy dependence of $\left\langle e^{i\mathbf{k}_{\parallel}\cdot\mathbf{r}_{\parallel}} \right| \mathbf{A}\cdot\mathbf{p} \left| \phi_i \right\rangle$ given by the W $5d$ photoionisation cross section as calculated by Yeh and Lindau [5]. The calculated spin polarisation is in good agreement with our measured photon energy-dependent spin polarisations (Fig. 2(i)). It validates our measurement of high photoelectron spin polarisations, confirming that we can selectively probe the top monolayer of the material, and that we can tune these by changing photon energy. The photon energy dependence of the calculated total intensity (Fig. S3) also well matches the variation in spectral weight of these bands from spin-integrated ARPES over an extended photon energy range. Together, these model

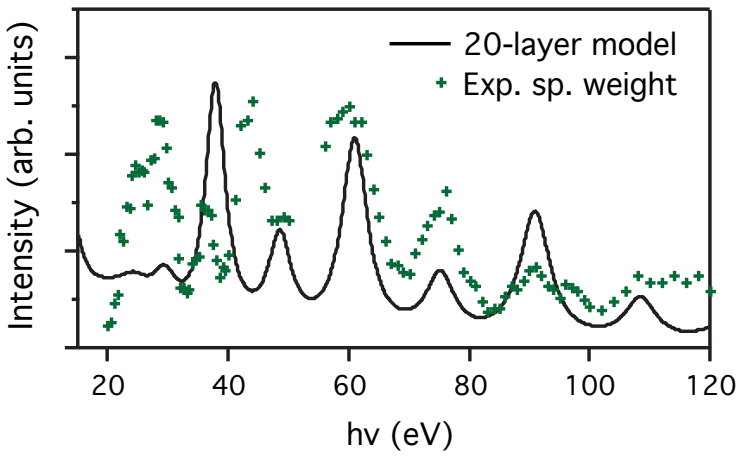

FIG. S3: **Photon energy dependence of spectral weight.** (a) Calculated (black line) total intensity predicted by the model described here, compared to the measured spectral weight of the upper valence band at the $\overline{K}$ point from spin-integrated ARPES (green points).

calculations and corresponding photon-energy dependent experimental measurements therefore strongly support our conclusions in the main text of an alternating layer-dependent spin texture in WSe_2 for a given valley index.

---

* To whom correspondence should be addressed: philip.king@st-andrews.ac.uk

[1] Gong, Z., *et al.* Magnetoelectric effects and valley-controlled spin quantum gates in transition metal dichalcogenide bilayers. *Nature Commun.* **4**, 2053 (2013).

[2] Zhu, Z.-H. *et al.* Layer-by-Layer Entangled Spin-Orbital Texture of the Topological Surface State in Bi_2Se_3. *Phys. Rev. Lett.* **110**, 216401 (2013).

[3] Zhu, Z.-H. *et al.* Photoelectron Spin-Polarization Control in the Topological Insulator Bi_2Se_3. *Phys. Rev. Lett.* **112**, 076802 (2014).

[4] Tanuma, S. Powell, C. J. and Penn, D. R. Calculations of electron inelastic mean free paths.. *Surf. Interface Anal.* **21**, 165 (1994).

[5] Yeh, J. J. and Lindau, I. Atomic subshell photoionization cross sections and asymmetry parameters: $1 \leq Z \leq 103$. *Atomic Data and Nuclear Data Tables* **32**, 1 (1985).